Journal of Magnetism and Magnetic Materials 557 (2022) 169481

Contents lists available at ScienceDirect

Journal of Magnetism and Magnetic Materials

journal homepage: www.elsevier.com/locate/jmmm

Research article

# Influence of phase boundary on magnetic and magnetocaloric properties of nanocrystalline $La_{0.17}Ca_{0.83}MnO_3$ sample

Nirmal Mondal [a], Soma Chatterjee [b], Kalipada Das [c,*], S. Kumar [a], I. Das [b]

[a] Physics Department, Jadavpur University, Kolkata 700032, India
[b] CMP Division, Saha Institute of Nuclear Physics, HBNI, AF-Bidhannagar, Kolkata 700064, India
[c] Department of physics, Seth Anandram Jaipuria College, 10-Raja Nabakrishna Street, Kolkata 700005, India

ARTICLE INFO

*Keywords:*
Manganites
Magnetocaloric effect
Nanocrystalline

ABSTRACT

In this present study we report the Magnetic properties and magnetocaloric effect of two nanocrystalline $La_{0.17}Ca_{0.83}MnO_3$ samples with average particle size ~40 nm and ~70 nm. According to the reported phase diagram, the bulk compound lies near the phase boundary between charge ordered antiferromagnetic and canted antiferromagnetic state. In contrast to the bulk counterpart, the significant effect of the phase boundary was observed on the physical properties of nanocrystalline compounds. Moreover, the signature of canted magnetic phase in nanocrystalline sample was probed through magnetocaloric effect study.

## 1. Introduction

From the last few decades, the physical properties of perovskite manganites $RMnO_3$ (R is trivalent rare earth ion such as La, Y, Pr, Gd etc.) were extensively studied . Among them, doped perovskite manganites $R_{1-x}B_xMnO_3$ (B is bivalent ion such as Ca, Sr, Ba etc.) exhibit much attention due to their variety of unusual interesting physical phenomena such as charge ordering, orbital ordering, metal–insulator transitions, colossal magnetoresistance (CMR), large magnetocaloric effect (MCE) etc. [1–10]. Moreover, strong correlation among magnetic, transport and structural properties are also seen in perovskite manganites [11–15]. Different kinds of magnetic states (ferromagnetic (FM), paramagnetic (PM), antiferromagnetic (AFM), canted antiferromagnetic (CAFM), spin glass (mixture of magnetic states), phase separation, phase coexistence etc.) present in these compounds. Some important interactions like double exchange (DE), Super exchange (SE), John's teller (JT), Coulomb interaction, and Hund's coupling can affect the physical properties of manganites due to the presence of complex electronic phases [16–19]. In manganites, some interesting phenomena originates because of the change of $Mn^{3+}$ and $Mn^{4+}$ ratio. $Mn^{4+}$ ion arises due to the addition of divalent chemical substitution with the trivalent rare earth ion. $La_{1-x}Ca_xMnO_3$ is mostly well studied compound among all of the perovskite manganites [20–25]. Depending upon the doping concentration of Ca, $La_{1-x}Ca_xMnO_3$ compound shows different types of magnetic phases. The end components $LaMnO_3$ and $CaMnO_3$ are in antiferromagnetic magnetic state [26–28]. With increasing x, the spins are trying to be canted and for the range $0 < x < 0.20$ canted antiferromagnetic state is observed. The region $0.50 < x < 0.87$ shows charge ordered (CO) state. Ferromagnetic metallic ground state occurs for the range $0.20 < x < 0.50$. Additionally, an insulating FM to metallic FM transformation is occurred at 50 K-150 K temperature and for T = 150 K–250 K ferromagnetic to paramagnetic transformation is observed. Ferromagnetic ground state is not observed in the $x > 0.5$ doping region. The region $0.5 < x < 0.87$ shows charge order transition where the transition temperature $T_{(CO)}$ is higher than previous $T_{(CO)}$($0.1 < x < 0.2$ region). Here, at low temperature ($T < 120$ K), the CO transition is followed by an antiferromagnetic transition. This charge order state disappears for $0.87 < x < 1.0$ and canted AFM state again originates at the low temperature region [29]. It is important to state that the phase boundaries mentioned above are not strictly clear because experimental observation shows that different phases may coexist and compete with each other [30–32]. The doping concentration x = 0.83 is in the region of CO state but it is situated near the phase boundary between CO-AFM and CAFM state. So, it is expected that some fraction of CAFM may appear in the charge order $La_{0.17}Ca_{0.83}MnO_3$ sample especially for the low dimensional systems. Canted magnetic states that developed due to the growth of antiferromagnetic correlation in its ferromagnetic state is associated with large value of magnetocaloric effect (MCE). Magnetocaloric effect study is an effective tool to understand the basic magnetic structure of an oxide system with complex interactions. It can also be used to probe phase coexistence and conversion in magnetic oxide systems [33–38]. Previously Biswas et al. reported the magnetocaloric effect of bulk $La_{0.17}Ca_{0.83}MnO_3$ sample and pointed out the negligible phase boundary effect for this compound [39]. In our present

* Corresponding author.
*E-mail address:* kalipadadasphysics@gmail.com (K. Das).

https://doi.org/10.1016/j.jmmm.2022.169481
Received 1 February 2022; Received in revised form 8 May 2022; Accepted 12 May 2022
Available online 20 May 2022

study, we have investigated magnetic and magnetocaloric properties of nanocrystalline $La_{0.17}Ca_{0.83}MnO_3$ sample for two different particle size (40 nm and 70 nm). AFM bulk compound can be converted into core–shell type nanocrystalline compound, where AFM state present in core and FM state in shell. It is well established that magnetic properties, magnetocaloric effect, magnetic phases can vary drastically with the reduction of particle size [40,41]. The physical properties of manganite compounds are modified not only by the chemical composition but also by the reduction of their particle size. In case of nanosized compounds, narrow grain size distribution was found to enhance the value of magnetocaloric effect. Compared to the bulk counterpart, the RC and RCP are greatly enhanced in case of nanoparticles [33,42–46]. In case of 40 nm sample, ferromagnetic transition is observed whereas for 70 nm sample FM nature is not noticed clearly but antiferromagnetic state remains coexist. The experimental outcome from magnetic measurement shows a weak signature of the coexistence of different magnetic state at low temperature region. However, such weak signature of magnetic phases clearly identified from the magnetocaloric effect study.

## 2. Sample preparation, characterizations and measurements

Nanocrystalline $La_{0.17}Ca_{0.83}MnO_3$ samples are prepared by well known sol–gel technique. Highly pure (99.99%) $CaCO_3$, and $MnO_2$ and preheated $La_2O_3$ are used as starting elements. At first, carbonates and oxides are converted into their nitrate form (using nitric acid with millipore water) to get clear solution. As $MnO_2$ is not soluble in nitric acid, required amount of oxalic acid is added to get clear solution. Then all the homogeneous solutions are taken in a large container and mixed up with a magnetic stirrer for 15 min. Required amount of citric acid are mixed up as a catalyst. Putting the solution container into a water bath, it was heated at 80–90 °C until the gel is formed. Then the sample is decomposed directly by a hot plate at 200–220 °C temperature and black porous powder formed. After palletizing the powder, the pallets are annealed at 800 °C and 1000 °C during 6 h for two nanocrystalline samples.

To estimate the average grain size from x-ray line width broadening, we have also prepared bulk counterpart by annealing the pellet at 1300 °C for 36 h. Room temperature x-ray diffraction (XRD) measurement was carried out to characterize the bulk as well as nanocrystalline compounds by using Rigaku- TTRAX-III diffractometer. Scanning electron microscope was used to determine average particle size of the nanoparticle. Magnetic and magnetocaloric effect was studied by using Super Conducting Interference Device (SQUID- VSM) within temperature range 2–300 K and magnetic field variation upto 70 kOe

## 3. Results and discussion

Room temperature x-ray diffraction measurements indicate the single phase nature of all the samples. Average particle size of nanocrystalline compound was estimated by using Scherrer's formula,

$$d = \frac{K\lambda}{\beta \cos\theta} \tag{1}$$

where K is a constant (~0.90) and $\lambda = 1.54$ Å is the wave length of the x-ray used for measurements. $\beta$ is the effective full width at half maxima (FWHM) for the maximum intense Bargg's peak which was corrected by the relation

$$\beta = B - \frac{b^2}{B} \tag{2}$$

Here 'b' and 'B' are the FWHM of a peak (measured at the same angle and same instrument) for bulk and nanocrystalline samples respectively. The estimated average particle sizes for the nanocrystalline samples are nearly 70 nm and 40 nm.

Room temperature x-ray diffraction pattern (along with profile fitting) for two nanocrystalline (70 nm and 40 nm) $La_{0.17}Ca_{0.83}MnO_3$ samples are shown in Fig. 1(a) and (b). Rietveld refinements are performed by using FULLPROF software package with Pnma space group symmetry. As no impurity peak is observed in XRD patterns, we can say that all the samples are in single-phase. The value of lattice parameters along with standard deviation and reliability factors of fitting for two nanocrystalline samples are listed in Table 1.

Scanning electron microscopy (SEM) images for two nanocrystalline samples are shown in Fig. 1(d) and (e). The particle size distribution is shown in the inset of Fig. 1(d) and (e). Interestingly, the estimated average particle sizes from SEM images are nicely matches with the calculated value measured from x-ray line width broadening. Energy Dispersive X-ray Analysis (EDX) indicate the formation of the sample in desired stoichiometry. The EDX patterns of the nanocrystalline compounds were depicted in Fig. 1.

It is well known that oxygen plays a crucial role in determining the physical properties of perovskite oxide materials and oxygen non-stoichiometry can influence the physical properties of the compounds [47,48]. In the present case, there is no significant change in transition temperatures in comparison to the previously reported articles of the bulk compound [39]. Hence, it may be assumed that oxygen non-stoichiometry is not significant in this case. Fig. 2(a) and (b) shows the variation of zero-field cooled (ZFC) and field cooled (FC) magnetization with temperature for 70 nm and 40 nm nanocrystalline $La_{0.17}Ca_{0.83}MnO_3$ samples respectively at H = 100 Oe magnetic field. For 70 nm nanocrystalline sample, Fig. 2(a) indicates that an antiferromagnetic behavior arises (T ~ 200 K) with the reduction of temperature and with further lowering the temperature a ferromagnetic like behavior appears. On the other hand, for 40 nm nanocrystalline sample, antiferromagnetic state was not observed, with lowering the temperature only ferromagnetic response arises (shown in Fig. 2(b)) similar as reported earlier [12]. Fig. 2(c) and (d) shows the temperature variation of magnetization at higher field value for 70 nm and 40 nm nanocrystalline samples respectively. In Fig. 2(c), only antiferromagnetic response was observed for 70 nm nanoparticle (ferromagnetic response was suppressed). In contrast to that, only ferromagnetic response was observed for 40 nm particle size sample (shown in Fig. 2(d)).

The variation of magnetization with external magnetic field (at temperature 5 K) for both nanocrystalline samples are shown in Fig. 3(a). For 40 nm nanocrystalline a hysteresis loop (with small width) was observed in M–H measurement which indicates about the ferromagnetic nature of the sample. Inset of the figure shows the enlarged view of hysteresis loop for this sample. While the 70 nm sample exhibits antiferromagnetic dominated nature with negligible hysteresis.

One quadrant M–H measurements were performed (to calculate magnetocaloric entropy change) for both nanocrystalline samples at different temperature, shown in Fig. 3(b) and (c) (for sake of clarity some selected isotherms are shown). Below the ordering temperature, the antiferromagnetic response was found (increasing magnetization with increasing temperature) for 70 nm nanocrystalline sample. However, the opposite mature (ferromagnetic nature) was found for 40 nm particle size sample.

It is well known that magnetocaloric effect is important for not only its application in environment friendly cooling technology but also it can be used as a powerful tool to probe any feeble magnetic transition [49–53]. Magnetocaloric effect can be defined by adiabatic temperature change or isothermal magnetic entropy change of magnetic materials due to the application of external magnetic field. Isothermal magnetic entropy change can be extracted from the magnetic field dependent magnetization by using Maxwell's thermodynamic relation

$$\Delta S = \int_0^H (\partial M/\partial T) dH \tag{3}$$

Regarding this context, it is worth mentioning that after each M–H measurement, the sample was warmed up to T = 300 K to remove the magnetic history if present. The magnetocaloric properties of the bulk

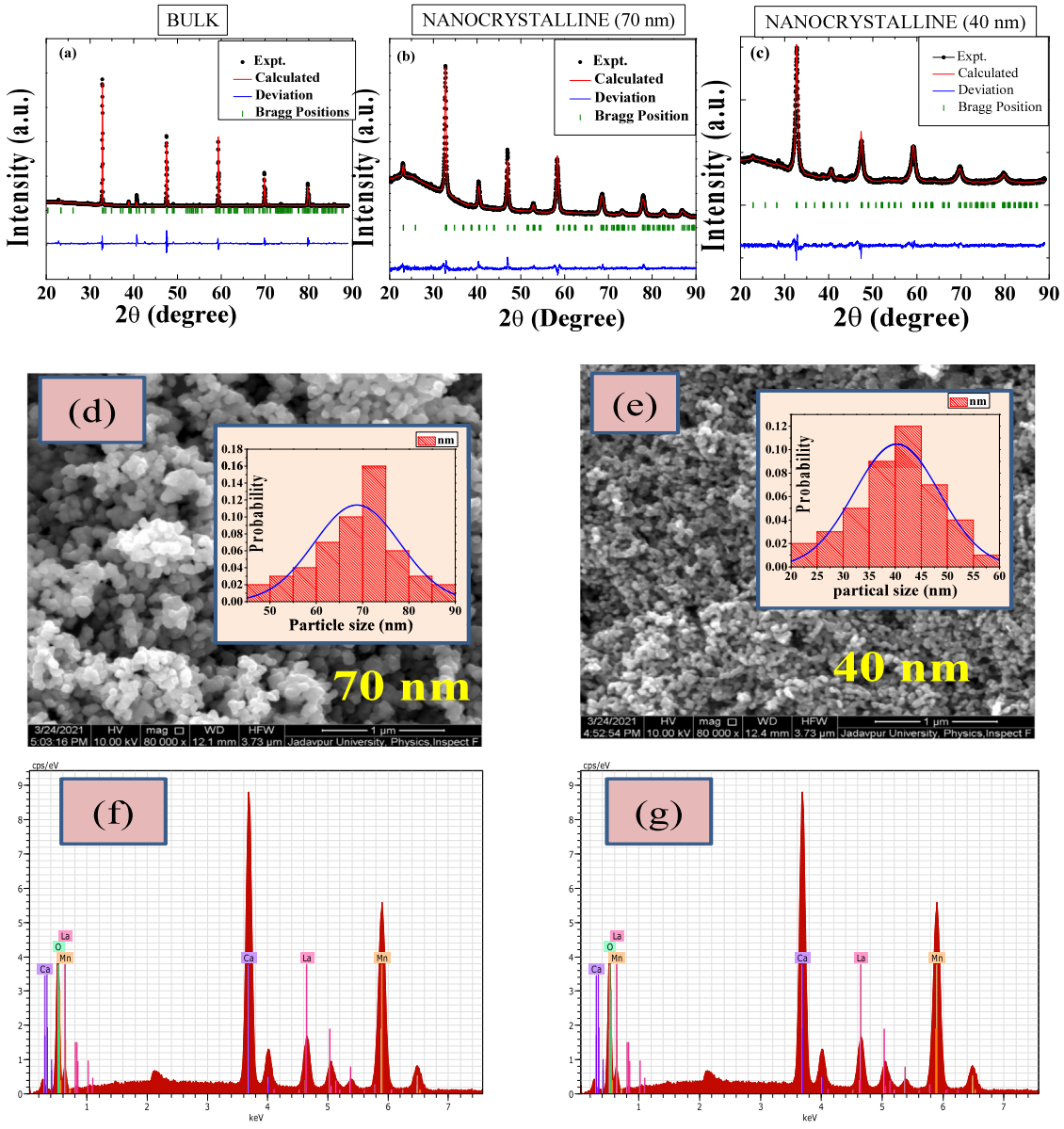


**Fig. 1.** Room temperature powder x-ray diffraction pattern (along with profile fitting) are shown in (a) bulk and (b) 70 nm nanocrystalline and (c) 40 nm nanocrystalline samples. (d), (e) represents the scanning electron microscopy images of 70 nm and 40 nm nanocrystalline samples respectively. (f) and (g) represents the Energy Dispersive X-ray Analysis (EDX) of 70 nm and 40 nm nanocrystalline samples respectively.

**Table 1**
Lattice parameters and reliability factors of fitting for 70 nm (LCMO-70) and 40 nm (LCMO-40) nanocrystalline samples.

| Compound | Space group | a (Å) | b (Å) | c (Å) | $\chi^2$ | $R_{WP}/R_{exp}$ |
|---|---|---|---|---|---|---|
| LCMO-70 nm | Pnma | 5.4743 ± 0.0004 | 5.5130 ± 0.0004 | 7.7783 ± 0.0007 | 2.03 | 1.42 |
| LCMO-40 nm | Pnma | 5.3516 ± 0.0007 | 5.3305 ± 0.0006 | 7.5289 ± 0.0009 | 2.15 | 1.46 |

$La_{0.17}Ca_{0.83}MnO_3$ sample is well documented in literature [39]. In our present study, we have calculated the magnetocaloric entropy change from isothermal M–H curves. Fig. 4(a) and (b) shows the variation of magnetic entropy change with temperature at different magnetic field values for 70 nm and 40 nm nanocrystalline $La_{0.17}Ca_{0.83}MnO_3$ samples respectively. The modification of the magnetocaloric properties with reduction of the particle size is reported earlier in several studies [54,55]. In the previous study it is well described that $-\Delta S$ vs. T graph shows a peak in the negative side (IMCE) for antiferromagnetic state whereas a positive peak appears (MCE) for ferromagnetic state. 70 nm particle sized sample shows a minimum of $-\Delta S$ (IMCE) at T ~ 160 K (similar as bulk counterpart) which is shown in Fig. 4(a). The negative value of $-\Delta S$ (IMCE) is the signature of antiferromagnetic transition for 70 nm nanoparticles. Here, we do not observe any other clear transition in the low temperature region .

In contrast to that, two clear peaks ($-\Delta S$ vs. T plot) with positive magnitude are observed for 40 nm particle sized sample which is shown in Fig. 4(b). Such positive peaks indicate the signature of ferromagnetic nature material. For charge ordered polycrystalline material, with the reduction of the particle size the AFM phase become weekend and a short-range FM correlation appears within the uncompensated surface spins [12,56]. Surface effect plays an important role to determine the properties of low dimensional nanocrystalline material. From the Fig. 4(a), it is clear that surface effect is not so enough to suppress

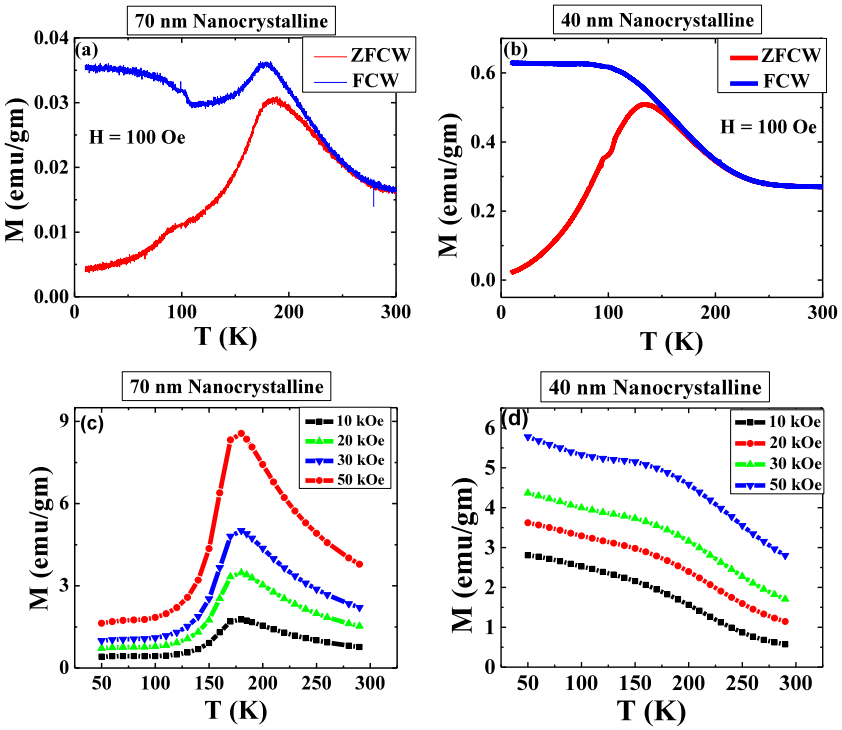


**Fig. 2.** (a), (b) represents temperature dependent magnetization measured at 100 Oe in ZFC and FC protocol for 70 nm and 40 nm nanoparticles respectively. (c), (d) shows the temperature dependent magnetization for several higher field values.

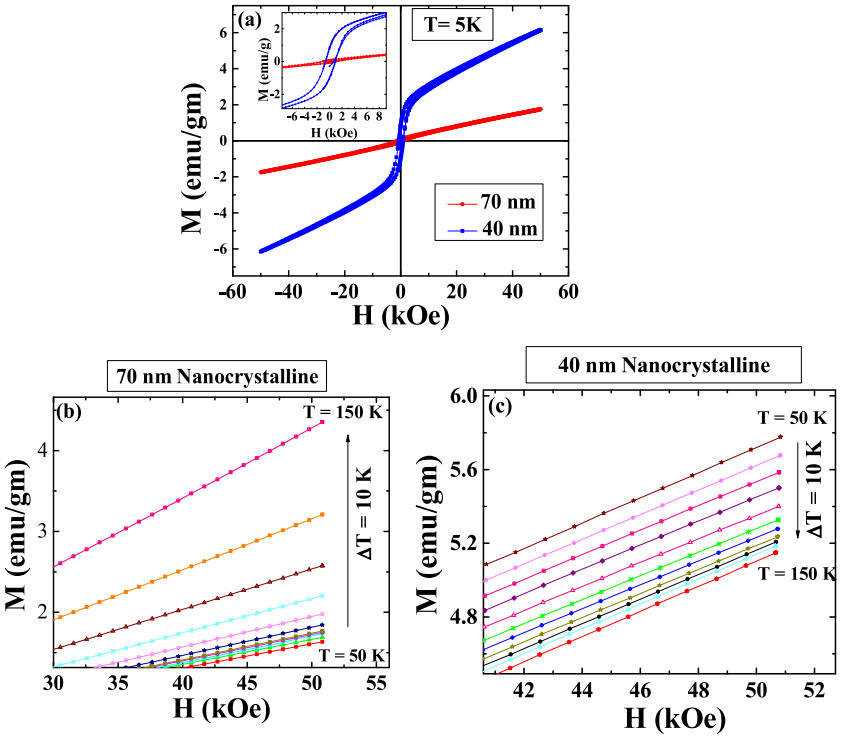


**Fig. 3.** (a) isothermal magnetization at 5 K for both 70 nm and 40 nm nanocrystalline samples and Inset shows the enlarged view of this curve the low field region for both the samples. One quadrant magnetization as a function of magnetic field at some selected temperature with 10 K interval is shown for (b) 70 nm and (c) 40 nm nanocrystalline $La_{0.17}Ca_{0.83}MnO_3$ samples.

the AFM signature completely for 70 nm nano material. However, for lower particle sized (40 nm) sample, surface effect plays a dominant role which is greatly reflected from its magnetocaloric properties. Moreover, the contribution related to the phase boundary effect become pronounced in case of the lower particle size sample. The existence of weak canted magnetic domains in the nanoparticles is manifested by a small peak at T = 75 K temperature. Regarding this context, it is worth mentioning that a very bare signature of such weak phase was also present in the 70 nm particle size sample. In the dc magnetization measurements, reflection of such weak magnetic phase was almost

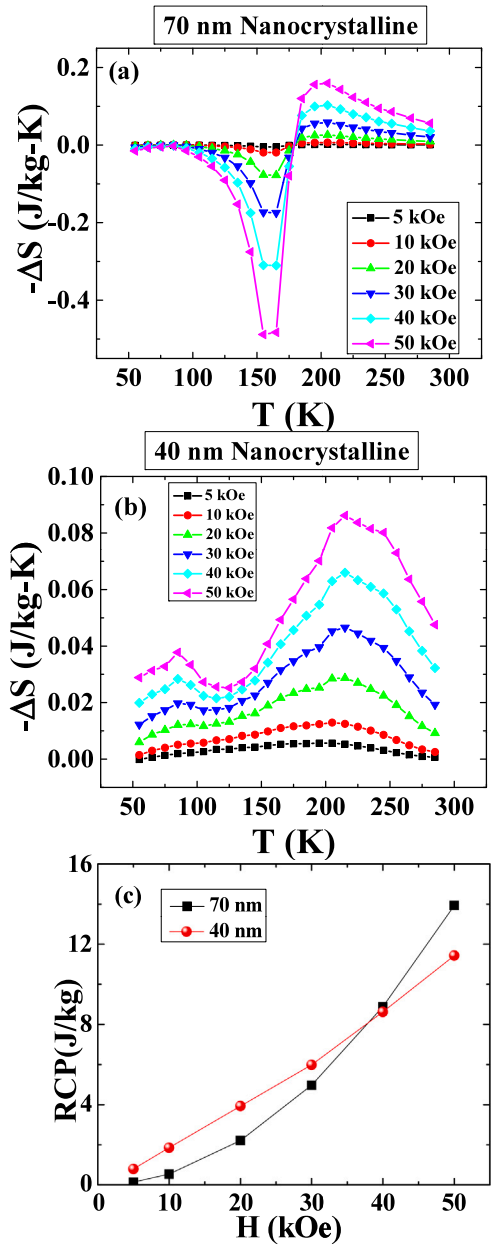


**Fig. 4.** Variation of magnetocaloric entropy change with temperature at different magnetic field for (a) 70 nm and (b) 40 nm nanoparticles. (c) Variation of relative cooling power (RCP) as a function of external magnetic field.

hidden within the predominant surface induced ferromagnetic environment for 40 nm particle size sample. On the other hand, in case of the 70 nm sample, antiferromagnetic signature is not diminished due to its larger particle size and small ferromagnetic signature present at very low field magnetization measurement (Fig. 2(a)). At higher external magnetic field values, the response of antiferromagnetic counterparts become substantially strong and the weak signature of canted ferromagnetic parts is suppressed.

Cooling capacity of a magnetic refrigerant material can be determined by using an important parameter called relative cooling power (RCP). Cooling capacity is related with the transfer of heat between hot source and cold sink in an ideal refrigeration cycle. The simplest method to calculate the value of RCP is given as

$$RCP = \Delta S^{max} \Delta T_{FWHM} \tag{4}$$

where $\Delta S^{max}$ is the maximum value of magnetic entropy change and $\Delta T_{FWHM}$ is the full width at half maxima of $\Delta S^{max}$. The variation of RCP with external magnetic field for both the compounds are also shown in Fig. 4(c). RCP value varies almost quadratically and linearly with the external magnetic field for 70 nm and 40 nm nanocrystalline samples respectively. In case of 70 nm nanocrystalline sample, RCP value is calculated by using inverse peak of the $-\Delta S(T)$ curve and the asymmetric nature of $-\Delta S(T)$ curve for this sample may lead the deviation of RCP (H) from the linear behavior.

From the Magnetization (M-T) and magnetocaloric effect ($-\Delta S(T)$) measurement, we have extracted almost identical critical parameters (transition temperature and critical magnetic field) that follows identical phase boundary. We have constructed magnetic phase diagram for both the $La_{0.17}Ca_{0.83}MnO_3$ nanocrystalline sample, which are shown in Fig. 5

Now, we have investigate the magnetic field dependence entropy change ($\Delta S$) corresponds to inverse magnetocaloric effect (IMCE) and conventional magnetocaloric effect (CMCE) for 70 nm and 40 nm $La_{0.17}Ca_{0.83}MnO_3$ nanocrystalline samples respectively. For any magnetocaloric material $\Delta S$ depends on H by using the following relation

$$\Delta S \sim H^n \tag{5}$$

'n' is an exponent that depends on both H,T for CMCE but independent for IMCE materials. The universal curve for IMCE (70 nm sample) can be obtained from $\Delta S/\Delta S^{max}$ vs. $T/T_P$ curve at different magnetic field values (where $\Delta S^{max}$ is the maximum value of magnetic entropy change and $T_P$ is the temperature correspond to peak). All the curves for this material fall into a single universal curve without rescaling the temperature axis (shown in Fig. 6(a)). However, for CMCE (40 nm sample) $\Delta S/\Delta S^{max}$ vs. $T/T_C$ ($T_C$ is curie temperature) curves does not collapse on a single universal curve (Fig. 6(b)). In case of CMCE material universal curve can be constructed by plotting $\Delta S/\Delta S^{max}$ vs. $\theta$ where $\theta$ is the temperature after rescaling the temperature axis by [57–59]

$$\theta = \frac{T - T_C}{T_r - T_C} \tag{6}$$

($T_r$ is the reference temperature). The values of $T_r$ are chosen for a certain fraction 'f' that satisfies the condition $f = \Delta S(T_r)/\Delta S(T_C)$ ($f = 0.8$ is used here).

## 4. Conclusions

In summary, we have studied the magnetic and magnetocaloric effect of two nanocrystalline $La_{0.17}Ca_{0.83}MnO_3$ samples. The different magnetic and magnetocaloric properties were observed depending on their particle sizes. For larger particle size sample (~70 nm), predominant antiferromagnetic part present in addition to the surface induced ferromagnetism. However, for lower particle size sample (~40 nm) the antiferromagnetic ground state is transformed into ferromagnetic state. Interestingly, in contrast to the bulk counterpart, the influence of the phase boundary become dominant at low temperature region when particle size is reduced. The response of the canted magnetic phase (hidden in dc magnetization measurements) was more clearly probed through the magnetocaloric effect study.

## Declaration of competing interest

The authors declare that they have no known competing financial interests or personal relationships that could have appeared to influence the work reported in this paper.

## Acknowledgments

The work was supported by Department of Atomic Energy (DAE), Govt. of India.

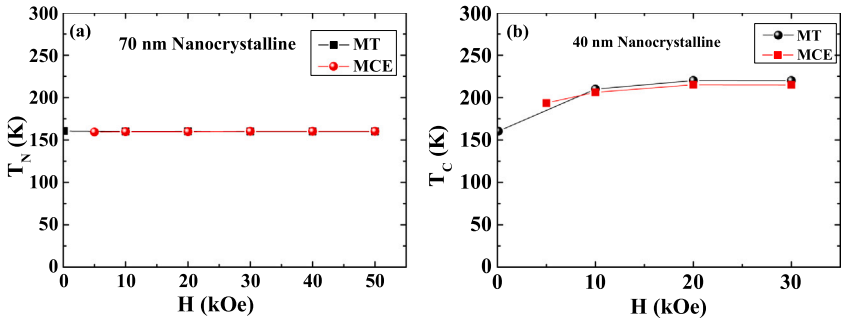


**Fig. 5.** Constructed magnetic phase diagram (critical parameters were extracted from the dc magnetization and magnetocaloric effect) for (a) 70 nm and (b) 40 nm nanoparticles.

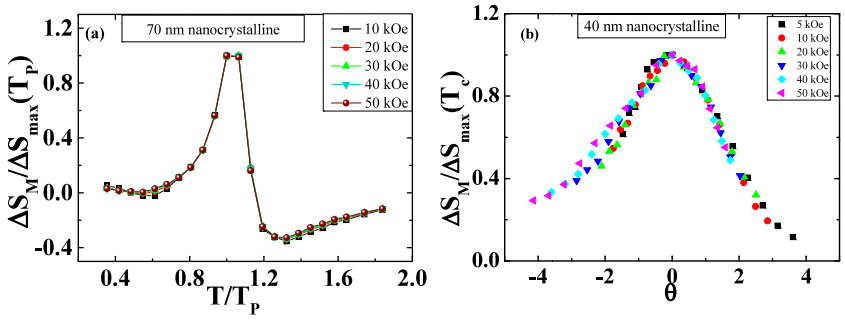


**Fig. 6.** Universal nature of the magnetocaloric entropy change for (a) 70 nm and (b) 40 nm nanoparticles.

## References


[1] Y. Tokura, Colossal Magnetoresistive Oxides, Gordon and Breach Science Publishers, The Netherlands, 2000.
[2] M.H. Phan, M.B. Morales, N.S. Bingham, H. Srikanth, C.L. Zhang, S.W. Cheong, Phys. Rev. B 81 (2010) 094413.
[3] A. Biswas, I. Das, Phys. Rev. B 74 (2006) 172405.
[4] S. Chandra, A.I. Figueroa, B. Ghosh, M.H. Phan, H. Srikanth, A.K. Raychaudhuri, J. Appl. Phys. 109 (2011) 07D720.
[5] Z.B. Guo, Y.W. Du, J.S. Zhu, H. Huang, W.P. Ding, D. Feng, Phys. Rev. Lett. 78 (1997) 1142.
[6] Z.B. Guo, J.R. Zhang, H. Huang, W.P. Ding, Y.W. Du, Appl. Phys. Lett. 70 (1996) 904.
[7] M.H. Phan, S.C. Yu, J. Magn. Magn. Mater. 308 (2007) 325.
[8] S. Jin, T.H. Tiefel, M. McCormack, R.A. Fastnacht, R. Ramesh, L.H. Chen, Science 264 (1994) 413.
[9] K. Das, R. Rawat, B. Satpati, I. Das, Appl. Phys. Lett. 103 (2013) 202406.
[10] K. Das, T. Paramanik, I. Das, J. Magn. Magn. Mater. 374 (2015) 707.
[11] Y. Tokura, Rep. Progr. Phys. 69 (2006) 797.
[12] S. Dong, F. Gao, Z.Q. Wang, J.M. Liu, Z.F. Ren, Appl. Phys. Lett. 90 (2007) 082508.
[13] Y. Tomioka, A. Asamitsu, H. Kuwahara, Y. Moritomo, Y. Tokura, Phys. Rev. B 53 (1996) R1689.
[14] Y. Okimoto, Y. Tomioka, Y. Onose, Y. Otsuka, Y. Tokura, Phys. Rev. B 57 (1998) R9377.
[15] K. Das, B. Satpati, I. Das, RSC Adv. 5 (2015) 27338.
[16] C. Zener, Phys. Rev. 81 (1951) 440.
[17] C. Zener, Phys. Rev. 82 (1951) 403.
[18] E. Pollert, S. Krupicka, E. Kuzwicova, J. Phys. Chem. Solids 43 (1982) 1137.
[19] G. Zhao, K. Conder, H. Keller, K.A. Muïller, Nature 381 (1996) 676.
[20] U. Shankar, A.K. Singh, J. Phys. Chem. C 119 (2015) 28620.
[21] C.H. Patterson, Phys. Rev. B 72 (2005) 085125.
[22] P. Levy, F. Parisi, G. Polla, D. Vega, G. Leyva, H. Lanza, R.S. Freitas, L. Ghivelder, Phys. Rev. B 62 (2000) 6437.
[23] T. Sarkar, B. Ghosh, A.K. Raychaudhuri, T. Chatterji, Phys. Rev. B 77 (2008) 235112.
[24] R.S. Freitas, L. Ghivelder, P. Levy, F. Parisi, Phys. Rev. B 65 (2002) 104403.
[25] G. Iniama, P. de la Presa, J.M. Alonso, M. Multigner, B.I. Ita, R. Cortés-Gil, M.L. Ruiz-González, A. Hernando, J.M. Gonzalez-Calbet, J. Appl. Phys. 116 (2014) 113901.
[26] Y. Tokura, N. Nagaosa, Science 288 (2000) 462.
[27] V.S. Su, et al., Phys. Rev. B 61 (2000) 1324.
[28] V. Spasojevic, D. Markovic, V. Kusigerski, B. Antic, S. Boskovic, M. Mitric, M. Vlajie, V. Krstic, B. Matovic, J. Alloys Compd. 442 (2007) 197.
[29] S.W. Cheong, H.Y. Hwang, in: Y. Tokura (Ed.), Contribution to Colossal Magnetoresistance Oxides, in: Monographs in Condensed Matter Science, Gordon and Breach, London, 1999.
[30] G. Matsumoto, J. Phys. Soc. Japan 29 (3) (1970) 606–615.
[31] A. Biswas, T. Samanta, S. Banerjee, I. Das, Appl. Phys. Lett. 94 (2009) 233109.
[32] A. Biswas, S. Chandra, T. Samanta, M.H. Phan, I. Das, J. Appl. Phys. 113 (2013) 17A902.
[33] S. Chandra, A. Biswas, S. Datta, B. Ghosh, V. Siruguri, A.K. Raychaudhuri, M.H. Phan, H. Srikanth, J. Phys.: Condens. Matter 24 (2012) 366004.
[34] R.P. Madhogaria, R. Das, E.M. Clements, V. Kalappattil, M.H. Phan, H. Srikanth, N.T. Dang, D.P. Kozlenko, N.S. Bingham, Phys. Rev. B 99 (2019) 104436.
[35] R.P. Madhogariaa, N.S. Binghamb, R. Dasc, M.H. Phana, H. Srikantha, J. Alloys Compd. 888 (2021) 161624.
[36] D.P. Kozlenko, N.T. Dang, R.P. Madhogaria, L.T.P. Thao, S.E. Kichanov, N. Tran, D.T. Khan, N. Truong-Tho, T.L. Phan, B.W. Lee, B.N. Savenko, A.V. Rutkaukas, L.H. Khiem, H.B. Nguyen, T.A. Tran, T. Kmječ, J. Kohout, V. Chlan, M.H. Phan, Phys. Rev. Mater. 5 (2021) 044407.
[37] P. Lampen-Kelleya, E.M. Clementsa, B. Casasa, M.H. Phana, H. Srikantha, J. Marcinb, I. Skorvanekb, H.T. Yic, S.W. Cheongc, J. Magn. Magn. Mater. 493 (2020) 165690.
[38] P. Lampen, N.S. Bingham, M.H. Phan, H. Srikanth, H.T. Yi, S.W. Cheong, Phys. Rev. B 89 (2014) 144414.
[39] A. Biswas, T. Samanta, S. Banerjee, I. Das, J. Phys.: Condens. Matter 21 (2009) 506005.
[40] S. Dong, R. Yu, S. Yunoki, J.-M. Liu, E. Dagotto, Phys. Rev. B 78 (2008) 064414.
[41] J.B. Goodenough, Phys. Rev. 100 (1955) 564.
[42] M. Pekala, V. Drozd, J. Non-Cryst. Solids 354 (2008) 5308.
[43] A. Biswas, S. Chandra, M.H. Phan, H. Srikanth, J. Alloys Compd. 545 (2012) 157.
[44] Y. Wang, J. Shao, Y. Yu, Q. Shi, Y. Zhu, T. Miao, H. Lin, L. Xiang, Q. Li, P. Cai, W. Wang, L. Yin, J. Shen, Phys. Rev. Mater. 3 (2019) 084411.
[45] T.L. Phan, T.D. Thanh, T.A. Ho, T.V. Manh, Q.T. Tran, P. Lampen, M.H. Phan, S.C. Yu, IEEE Trans. Magn. 50 (2014) 11.
[46] S. Chandra, A. Biswas, M.H. Phan, H. Srikanth, J. Magn. Magn. Mater. 384 (2015) 138.
[47] V.Y. Mitrofanova, S.K. Estemirovaa, G.A. Kozhinaa, J. Magn. Magn. Mater. 476 (2019) 199.
[48] N.A. Liedienov, V.M. Kalita, A.V. Pashchenko, Y.I. Dzhezherya, I.V. Fesych, Q. Li, G.G. Levchenko, J. Alloys Compd. 836 (2020) 155440.
[49] A.M. Tishin, Y.I. Spichkin, The Magnetocaloric Effect and its Applications, Institute of Physics Publishing, Bristol and Philadelphia, 2003.
[50] K.A. Gschneidner Jr., V.K. Pecharsky, A.O. Tsokol, Rep. Progr. Phys. 68 (2005) 1479.
[51] T. Samanta, I. Das, S. Banerjee, Appl. Phys. Lett. 91 (2007) 152506.

[52] T. Samanta, A.U. Saleheen, D.L. Lepkowski, A. Shankar, I. Dubenko, A. Quetz, M. Khan, N. Ali, S. Stadler, Phys. Rev. B 91 (2014) 064412.
[53] K. Das, I. Das, J. Appl. Phys. 119 (2016) 093903.
[54] A. Rostamnejadi, M. Venkatesan, J. Alaria, M. Boese, P. Kameli, H. Salamati, J.M.D. Coey, J. Appl. Phys. 110 (2011) 043905.
[55] W.J. Lu, X. Luo, C.Y. Hao, W.H. Song, Y.P. Sun, J. Appl. Phys. 104 (2008) 113908.
[56] K. Das, S. Mandal, D. Mazumdar, P. Sen, I. Das, J. Magn. Magn. Mater. 501 (2020) 166421.
[57] A. Biswas, S. Chandra, T. Samanta, B. Ghosh, S. Datta, M.H. Phan, A.K. Raychaudhuri, I. Das, H. Srikanth, Phys. Rev. B 87 (2013) 134420.
[58] A. Biswas, T.L. Phan, N.H. Dan, P. Zhang, S.C. Yu, H. Srikanth, M.H. Phan, Appl. Phys. Lett. 103 (2013) 162410.
[59] A. Biswas, S. Chandra, T. Samanta, M.H. Phan, I. Das, J. Appl. Phys. 113 (2013) 17A902.